Hamed Kaghazchi ✉
Mustafa Kerem Ün

https://doi.org/10.21278/TOF.482050023
ISSN 1333-1124
eISSN 1849-1391

INVESTIGATION OF THE EFFECT OF CONDUCTIVITY CHANGES OF ISCHEMIC HEART TISSUE ON THE ST SEGMENT OF ELECTROCARDIOGRAPHY USING THE FINITE ELEMENT METHOD

Summary

Electrocardiography is a commonly used diagnostic method based on reading electrical potentials on the human torso. Ischemia is a common pathology diagnosed with electrocardiography and also the subject of many forward and inverse simulation studies. In these studies, ischemia is usually modelled by imposing an unhealthy transmembrane potential on the diseased region without taking the associated change in electrical conductivity of the ischemic tissue into account. Our objective in this paper is to investigate numerically the effect of ischemic conductivities imposed on the ischemic region on the outcome of the forward electrocardiography problem of simulation of the ischemic heart. To achieve this objective, a finite element code was written to solve the bidomain problem on realistic thorax geometries with inhomogeneous and anisotropic conductivities. The geometric model for this study consists of a single two-dimensional slice of MRI data available from the University of Utah resources. Realistic conductivities are assigned to healthy and ischemic tissues which are refined to achieve higher spatial density in order to improve numerical solution accuracy. The results show that taking into account ischemic conductivity may significantly change the estimated torso potentials in the forward analysis. We conclude that ischemic heart tissue should be simulated not only by imposing an unhealthy transmembrane potential but also unhealthy conductivities in numerical studies to achieve a more accurate simulation of this pathology.

Key words: *bidomain heart, ischemic tissue, finite element method, conductivity, forward problem*

1. Introduction

The electrical activity of the heart is essential for its functioning. Mathematical modelling of the heart's electrical activity from cell level to tissue level has been a major research topic for several decades.

Calculating the electrical field throughout the body arising from a cardiac source is known as the forward problem of electrocardiography (ECG). The solution to the forward problem allows researchers to predict the effect of various factors (such as geometry, inhomogeneity, and anisotropy) on epicardial potentials and on body potentials [1].

Ischemia is a relatively common heart condition caused by an insufficient oxygen supply to the heart muscle due to reduced blood flow to the tissue. It is usually caused by partially or totally clogged coronary arteries. Depending on where the blood flow is reduced in the heart, it can occur in the anterior or posterior ventricular walls. Since it is a progressive pathology, the ischemic region may grow in size. The clinical sign of acute myocardial ischemia is a shift of the ST segment of the ECG relative to the normal, whose magnitude depends on the size and location of the ischemic region in the heart tissue, as well as on the severity of the ischemia. In clinical practice, ECG has modest sensitivity and specificity (65-80%) in detecting and localising myocardial ischemia [2, 3].

Determining the size and the location of the ischemic region in the heart from the measured body surface potentials represents an inverse problem and has been a major focus of numerical studies concerning conduction in the heart. The finite element method (FEM) is widely utilised in forward and inverse problem simulations [4-6].

In a healthy heart, the whole heart muscle is in a depolarised state with a plateau transmembrane potential (TMP) of 0 mV during the ST segment of the ECG. On the other hand, in the case of ischemia, an abnormal TMP of -30 mV is observed in the tissue. FEM simulations of ischemia are usually performed during the ST segment of the cardiac cycle where the heart is considered to be at a momentary steady state. This effectively eliminates time as a variable from the problem and greatly reduces the problem's complexity. Ischemia is generally simulated only by imposing the abnormal TMP -30 mV on the ischemic region in the heart [2], [7]. However, the altered electrical conductivity associated with ischemia has usually been disregarded in simulation studies until recently [8, 9]. The effect of altered conductivity has never been systematically evaluated.

The goal of this numerical study is to investigate the effect of the conductivity change in ischemic heart tissue on the resulting torso surface potentials during the ST segment of the FEM simulation of the forward ECG problem. The effect of anisotropy of healthy and ischemic conductivities is also evaluated in comparison to assumed isotropic conductivities.

2. Method

2.1 Bidomain model of the heart

In the bidomain model of the heart, the intracellular and extracellular media of the heart muscle is considered as separate, overlapping, but interacting continua. Letting Φ_i and Φ_e denote the intracellular and extracellular potentials, respectively, the TMP potential across the cell membrane is given by

$$V_m = \Phi_i - \Phi_e \tag{1}$$

Both potentials satisfy the Poisson equation:

$$\nabla \cdot (\boldsymbol{\sigma}_i \nabla \Phi_i) = A_m I_m \tag{2}$$

$$\nabla \cdot (\boldsymbol{\sigma}_e \nabla \Phi_e) = -A_m I_m \tag{3}$$

Here, A_m is the surface-to-volume ratio of the cell membrane and I_m is the transmembrane current density per area [10]. The conductivity tensors of intracellular and extracellular domains, $\boldsymbol{\sigma}_i$ and $\boldsymbol{\sigma}_e$ respectively, express the anisotropic conductivity tensors in the heart muscle. Equations (1-3) can be combined into one as:

$$\nabla \cdot ((\boldsymbol{\sigma}_i + \boldsymbol{\sigma}_e) \nabla \Phi_e) = -\nabla \cdot (\boldsymbol{\sigma}_i \nabla V_m) \tag{4}$$

Equation (4) is the first of the two bidomain equations.

The current density across the membrane I_m may be described by a time-dependent capacitive current and ionic current

$$I_m = C_m \frac{\partial V_m}{\partial t} + I_{ion} \tag{5}$$

where C_m is the capacitance per unit area of the membrane and I_{ion} is the ionic current.

Substituting equation (1) and equation (5) into equation (2) to eliminate Φ_i gives

$$\nabla \cdot (\boldsymbol{\sigma}_i \nabla V_m) + \nabla \cdot (\boldsymbol{\sigma}_i \nabla \Phi_e) = A_m (C_m \frac{\partial V_m}{\partial t} + I_{ion}) \tag{6}$$

Equation (6) is the second of the bidomain equations [11, 12].

During the ST phase, the time derivative and the net ion flux I_{ion} in equation (6) vanish, and the bidomain model reduces to equation (4) since equation (6) becomes redundant.

The torso is a passive isotropic conductor surrounded by air where the potential within the torso region Φ_T satisfies the Laplace Equation:

$$\nabla \cdot (\sigma_T \nabla \Phi_T) = 0 \tag{7}$$

with σ_T indicating the isotropic conductivity of the non-heart torso tissue (lungs, fat, skeletal muscle, blood or torso cavity depending on the considered domain point). The continuity of potential and current density, respectively, across the torso-heart interface (i.e. outer surface of the heart) requires:

$$\Phi_e = \Phi_T \tag{8}$$

$$(\boldsymbol{\sigma}_e \nabla \Phi_e) \cdot \mathbf{n}_H = -(\sigma_T \nabla \Phi_T) \cdot \mathbf{n}_H \tag{9}$$

where $\mathbf{n}_H$ indicates the unit outward normal vector perpendicular to the heart-torso interface.

The applied reference voltage in ECG translates to a Dirichlet boundary condition on part of the torso's outer boundary as

$$\Phi_T = \Phi_0 \tag{10}$$

The torso is surrounded by air and no current can flow out of it, which is a Neumann boundary condition and can be expressed as:

$$(\sigma_T \nabla \Phi_T) \cdot \mathbf{n}_T = 0 \tag{11}$$

where $\mathbf{n}_T$ is the outward normal of the torso.

Let $\boldsymbol{x}$ symbolise the point coordinates in the problem domain. Indicating the heart domain with H and the torso with T, the associated outer boundaries with "∂" and the entire problem domain with $\Omega = T \cup H$, the model can be summarised as follows:

$$-\nabla \cdot (\boldsymbol{\sigma}(\boldsymbol{x}) \nabla \Phi(\boldsymbol{x})) = f(\boldsymbol{x}), \qquad \boldsymbol{x} \in \Omega \tag{12}$$

$$f(\boldsymbol{x}) = \begin{cases} 0, & \boldsymbol{x} \in T \\ \nabla \cdot (\boldsymbol{\sigma}_i \nabla V_m(\boldsymbol{x})), & \boldsymbol{x} \in H \end{cases} \tag{13}$$

where

$$\Phi(\boldsymbol{x}) = \begin{cases} \Phi_T & \boldsymbol{x} \in T \\ \Phi_e & \boldsymbol{x} \in H \end{cases} \tag{14}$$

$$\boldsymbol{\sigma}(\boldsymbol{x}) = \begin{cases} \sigma_T \mathbf{I} & \boldsymbol{x} \in \boldsymbol{T} \\ \boldsymbol{\sigma_i} + \boldsymbol{\sigma_e} & \boldsymbol{x} \in \boldsymbol{H} \end{cases} \tag{15}$$

and where $\mathbf{I}$ is the 2×2 identity matrix

$$(\sigma_T \nabla \Phi_T) \cdot \mathbf{n}_T = 0, \qquad \text{on } \partial T \tag{16}$$

$$\Phi_e = \Phi_T, \qquad \text{on } \partial H \tag{17}$$

$$(\boldsymbol{\sigma}_e \nabla \Phi_e) \cdot \mathbf{n}_H = -(\sigma_T \nabla \Phi_T) \cdot \mathbf{n}_H, \quad \text{on } \partial H \tag{18}$$

In this work, we model the torso including the heart as a two-dimensional medium and solve the two-dimensional version of the bidomain problem using the FEM. We preferred a two-dimensional computational study rather than a three-dimensional analysis to reduce the computational complexity of the problem. Important conclusions can still be drawn from two-dimensional simulations [13] and this approach is still encountered in the literature [14].

2.2 Finite element formulation of the bidomain heart

The finite element formulation used is based on the standard Galerkin formulation and is summarised here for completeness. The reader is referred to other sources for further details of this formulation [2], [5], [15]. The weighted residual of equation (12) over the problem domain is expressed as:

$$\int_T \left[\nabla \cdot (\sigma_T \nabla \Phi_T)\right] w \, \mathrm{d}\Omega = 0 \tag{19}$$

for the torso and

$$\int_H \left[\nabla \cdot ((\boldsymbol{\sigma}_i + \boldsymbol{\sigma}_e) \nabla \Phi_e) + \nabla \cdot (\boldsymbol{\sigma}_i \nabla V_m)\right] w \, \mathrm{d}\Omega = 0 \tag{20}$$

for the heart region, with w indicating the weighting function. Using tensorial identities and the Green-Gauss theorem on both equations (19-20) yields:

$$\int_T (\sigma_T \nabla \Phi_T) \cdot \nabla w \, \mathrm{d}\Omega - \int_{\partial T} w (\sigma_T \nabla \Phi_T) \cdot \mathbf{n}_T \, \mathrm{d}\Gamma + \int_{\partial H} w (\sigma_T \nabla \Phi_T) \cdot \mathbf{n}_H \, \mathrm{d}\Gamma = 0 \tag{21}$$

$$\int_H ((\boldsymbol{\sigma}_i + \boldsymbol{\sigma}_e) \nabla \Phi_e) \cdot \nabla w \, \mathrm{d}\Omega - \int_{\partial H} w ((\boldsymbol{\sigma}_i + \boldsymbol{\sigma}_e) \nabla \Phi_e) \cdot \mathbf{n}_H \mathrm{d}\Omega = -\int_H (\boldsymbol{\sigma}_i \nabla V_m) \cdot \nabla w \, \mathrm{d}\Omega \tag{22}$$

where $\partial\Gamma$ indicates the differential boundary element. We assume that the ischemic region does not directly interface with the torso. When equations (21-22) are summed up and equations (16), (18) are utilised, all boundary integrals vanish. (Note that the torso region has two boundaries ∂T and ∂H):

$$\int_H ((\boldsymbol{\sigma}_i + \boldsymbol{\sigma}_e) \nabla \Phi_e) \cdot \nabla w \, \mathrm{d}\Omega + \int_T (\sigma_T \nabla \Phi_T) \cdot \nabla w \, \mathrm{d}\Omega = \int_H (\boldsymbol{\sigma}_i \nabla V_m) \cdot \nabla w \, \mathrm{d}\Omega \tag{23}$$

The above formula prescribes basically a FEM formulation for the Poisson problem with inhomogeneous conductivities. It should also be noted that the right-hand side of equation (23) takes a nonzero value around the boundary of the ischemic zone in the heart and acts as the source term. The integrals in equation (23) are the sum of individual integrals evaluated over the M and L elements in the heart and the torso, respectively:

$$\sum_{k=1}^{M} \int_{H_k} ((\boldsymbol{\sigma}_i + \boldsymbol{\sigma}_e) \nabla \Phi_e) \cdot \nabla w \, \mathrm{d}\Omega_k + \sum_{k=1}^{L} \int_{T_k} (\sigma_T \nabla \Phi_e) \cdot \nabla w \, \mathrm{d}\Omega_k = -\sum_{k=1}^{M} \int_{H_k} (\boldsymbol{\sigma}_i \nabla V_m) \cdot \nabla w \, \mathrm{d}\Omega_k \tag{24}$$

Assuming a total of J nodes in the entire mesh, Φ and w are interpolated on both regions using the nodal shape functions $N_j(\boldsymbol{x})$ as:

$$\Phi_e = \sum_{j=1}^{M} c_j N_j = \mathbf{N}\mathbf{c} \tag{25}$$

$$w = \sum_{j=1}^{M} d_j N_j = \mathbf{N}\mathbf{d} \tag{26}$$

where **N** is the row vector containing the nodal shape functions, and the column vectors **c** and **d** contain the nodal degrees of freedom. The source term creates a force vector **f** with nonzero entries corresponding to the heart nodes where ∇V_m is nonzero. Equations (21-22), when substituted into equation (20), result in a system in the form:

$$\mathbf{d}^T(\mathbf{Kc}-\mathbf{f})=\mathbf{0} \tag{27}$$

where **K** is the stiffness matrix and **f** is the force vector. The vector **d** is assumed to be arbitrary, and the above equality holds if

$$\mathbf{Kc}=\mathbf{f} \tag{28}$$

The solution of equation (24) gives the vector **c** and produces the FEM solution to the problem.

2.3 Material properties of heart tissue

The anisotropy of the heart muscle is a consequence of its fibrous structure. The conductivity is higher parallel to the fibres compared to the cross-fibre direction [4], [16]. Furthermore, the muscle fibres are organised in sheets. Consequently, it is possible to define local principal directions of anisotropy at any point within the myocardium according to this structure. In two dimensions, the first principal direction is along the fibre direction (fibre axis) and the second one is perpendicular to the fibre axis lying in the sheet plane (sheet axis) [17]. In this local coordinate system, the conductivity tensor σ* is diagonal and is given as:

$$\boldsymbol{\sigma}^*=\begin{bmatrix}\sigma_l & 0\\ 0 & \sigma_t\end{bmatrix} \tag{29}$$

where σ_l and σ_t are conductivities parallel and perpendicular to the fibre, respectively. In the FEM formulation, the conductivity given in the local coordinates needs to be transformed to the Cartesian coordinates [18, 19]. In two dimensions, if the local coordinates system has a positive (clockwise) rotation of θ with respect to the Cartesian coordinates, the conductivity tensor is transformed to the Cartesian coordinates as:

$$\boldsymbol{\sigma}_h=\mathbf{A}\boldsymbol{\sigma}_h^*\mathbf{A}^T \quad h=i \text{ or } e \tag{30}$$

where $\boldsymbol{\sigma}_h$ is the conductivity tensor of either the intracellular (i) or extracellular (e) medium, and the matrix A is an orthogonal rotation matrix given by

$$\mathbf{A}=\begin{bmatrix}\cos\theta & \sin\theta\\ -\sin\theta & \cos\theta\end{bmatrix} \tag{31}$$

Using the generalised helicoid model (GHM) [20-22] given in the literature, the fibre orientation can be expressed with an orientation function $\theta(x, y)$ in two dimensions expressed as:

$$\theta(x,y)=\tan^{-1}\left(\frac{K_T x+K_N y}{1+K_N x-K_T y}\right) \tag{32}$$

where $K_T = 0.3$ and $K_N = 0.2$ are the GHM constants [21].

It is known that, during the action potential, the transmembrane potential jumps from a value of -90 mV to close to 0 mV for healthy tissue, but may reach only -30 mV in the case of ischemia. It is also known that both intracellular and extracellular conductivity values decrease in the case of ischemia or more severe lesions [7], [23]. In this work, the conductivity values for ischemic and healthy tissues taken from the literature (Table 1) [24] are used in the FEM simulation.

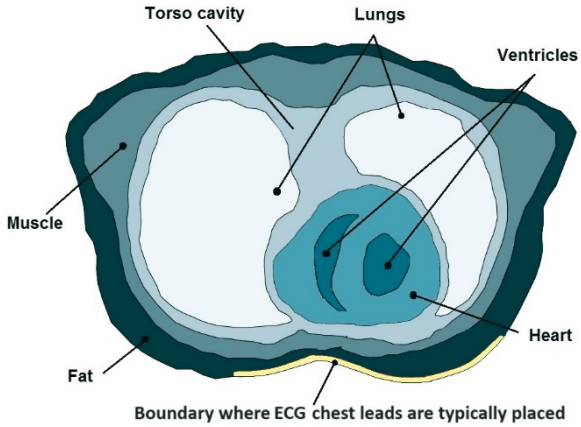

Fig. 1 Two-dimensional geometric model of the torso. The marked boundary on the chest indicates the location where the ECG chest leads are placed.

Table 1 Longitudinal (σ_l) and transverse (σ_t) values (see equation (29)) of anisotropic intracellular ($\boldsymbol{\sigma}_i$) and extracellular ($\boldsymbol{\sigma}_e$) conductivities of healthy and ischemic tissues

Conductivity component	**Value** (mS/cm)
Healthy intracellular longitudinal	3.000
Healthy intracellular transverse	0.315
Healthy extracellular longitudinal	2.000
Healthy extracellular transverse	1.351
Ischemic intracellular longitudinal	0.300
Ischemic intracellular transverse	0.006
Ischemic extracellular longitudinal	1.000
Ischemic extracellular transverse	1.010

2.4 Geometric model

The geometric model for this study consisted of a single two-dimensional slice of MRI data obtained from the University of Utah resources [4], [13], [25]. The slice image is taken 50 mm superior to the apex of the heart, a level that cuts through the ventricular walls where ischemia is most common and in line with the ECG chest leads. The image is processed for the segmentation of lungs, skeletal muscle, fat, and the torso cavity (Fig. 1). Different isotropic conductivity values are assigned to these regions (Table 2) [13], [26-27].

Table 2 Conductivity values (indicated as σ_T in the FEM formulation) corresponding to different non-heart tissues in the model

Tissue	**Conductivity** (mS/cm)
Lungs	0.96
Skeletal Muscle	2.00
Fat	0.45
Blood	2.39
Torso Cavity	2.39

2.5 Modelling of the ischemic region

A healthy heart is electrically inactive during the ST phase. Hence, the ST segment of the ECG is on the baseline level. However, in the presence of ischemia, a difference in the TMP between the ischemic and healthy tissue occurs which results in the shift of the ST segment from the baseline. The magnitude and direction of the ST shift and the ECG leads where the shift is observed are indicative of the size and location of the ischemic region. However, diagnosing ischemia and infarction is far from simple [27-29].

Since we are interested in modelling only the ST-segment shift, we take advantage of the fact that during the ST interval the TMP is homogeneous throughout the heart except for the ischemic tissue [27]. Consequently, the TMP is defined as:

$$V_m(x,y)=\begin{cases} 0\ \text{mV}, & \text{for healthy tissue} \\ -30\ \text{mV}, & \text{for ischemic tissue} \end{cases} \tag{33}$$

When implementing equation (33), the transition from healthy tissue to diseased tissue occurs not abruptly but through a transition zone. Clearly, the size of the transition zone and the profile of V_m across this zone (i.e. the magnitude of the source) will affect ∇V_m and the problem outcome. We defined a strip of thickness h of the ischemic region next to the healthy region as the transition zone and proposed the following functional variation within this zone:

$$V_m = 30\cdot\cos\left(\frac{\pi d}{h}\right)-30 \tag{34}$$

where h is the width of the transition zone, which varies between 0.4 – 1 mm [30]. d is the perpendicular distance of the considered point to the border of the ischemic region. Therefore, equation (30) can be written in the form:

$$V_m(d)=\begin{cases} 0, & \text{for } \Omega_{Healthy} \\ 30\cdot\cos\left(\frac{\pi d}{h}\right)-30, & \text{for } \Omega_{Transition} \\ -30, & \text{for } \Omega_{Ischemic} \end{cases} \tag{35}$$

where Ω_{Healthy}, Ω_{Ischemic} and $\Omega_{\text{Transition}}$ indicate healthy and ischemic tissues and the transition zone of the heart, respectively.

2.6 Programming of the finite element code

To solve the forward problem of ECG, we programmed a FEM code from scratch in Python language using the Spyder environment. The code is designed in such a way that it can solve both the Poisson and Laplace PDEs in the appropriate parts of the problem domain simultaneously. In addition, different conductivity tensors can be assigned to different elements according to equation (28) and equation (29). These features are not typically available in commercial finite element packages. The code was validated by comparing its results with those obtained from the COMSOL Multiphysics (COMSOL AB, Stockholm, Sweden) package in certain test problems. The finite element mesh of the geometric model was also generated using COMSOL.

3. Results

Three different ischemia cases, each with an ischemic region of a different size and location, are created within the geometric model. The ischemia cases represent realistic scenarios and we will refer to them as “Ischemia 1”, “Ischemia 2”, and “Ischemia 3”. A membrane potential of -30 mV along with the appropriate conductivity values is imposed on the ischemic regions to simulate ischemia.

The examples are run with isotropic and (more realistic) anisotropic conductivities both in the healthy heart and in the ischemic region. For both healthy and ischemic tissues, the isotropic conductivities are taken to be equal to the longitudinal conductivity values given in Table 1. The resulting potentials are compared with those obtained with healthy conductivities

imposed on the whole heart including the ischemic region. (Recall that, in the existing literature, ischemia is imposed only through ischemic TMP, and conductivity change originating from ischemia is usually ignored.)

The simulated potentials are observed along a boundary line in the chest that corresponds to the locations of pericardial (chest) leads of ECG (Fig. 1), which is also indicated in Figs. 2, 5, and 8 which describe the above-mentioned three ischemia cases. The mesh nodes that coincide with this boundary line are numbered from left to right, which we refer to as the "node index". In the graphs displayed in the figures below, the torso potentials are plotted against the node index.

In the first example (Ischemia 1, Fig. 2), the results show that taking ischemic conductivity into account increases the magnitude of the measured torso potentials both in the isotropic case (Fig. 3) and in the anisotropic case (Fig. 4). The difference seems significant in the anisotropic case.

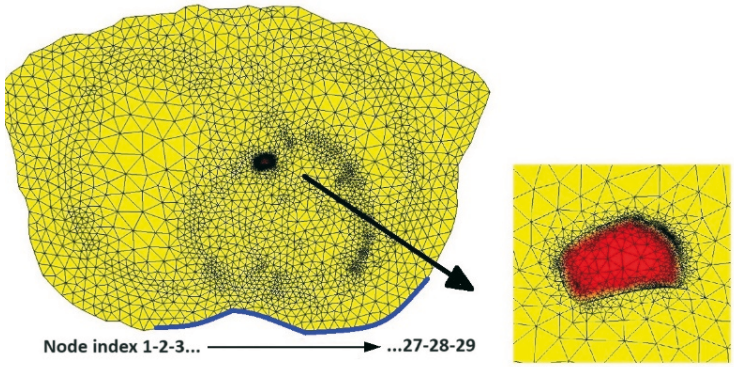

Fig. 2 Torso model and ischemic region on the posterior wall of the heart (Ischemia 1). The torso potential results are displayed for the nodes located along the chest boundary line (dark line) as a function of the node index.

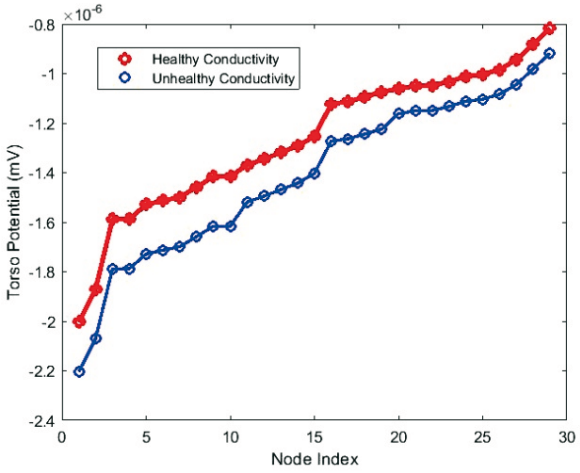

Fig. 3 Torso potentials predicted at the epicardial nodes with isotropic heart tissue using healthy and unhealthy (ischemic) conductivities (Ischemia 1).

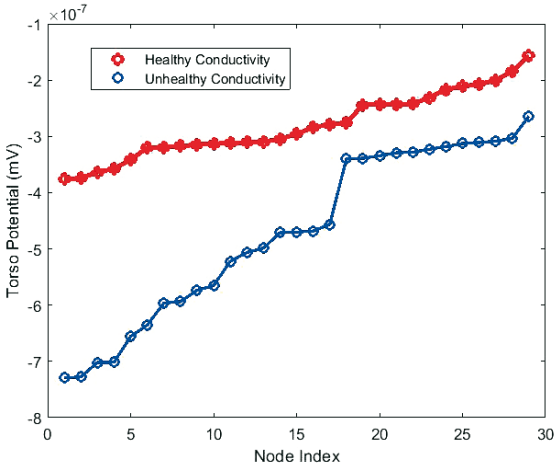

Fig. 4 Torso potentials predicted at the chest nodes with anisotropic heart tissue using healthy and unhealthy (ischemic)conductivities (Ischemia 1).

In the next example (Ischemia 2, Fig. 5), an ischemic region is created again in the left ventricle but closer to the posterior side of the chest. A similar comparison is made as in the first example. Since the ischemic region in this example is closer to the nodes where the torso potentials are measured, the measured potentials are larger in magnitude. Taking the ischemic conductivity into account seems to make a difference in this example as well. While the difference in the measured potentials is relatively small in the isotropic case (Fig. 6), it is significantly higher in the anisotropic case (Fig. 7).

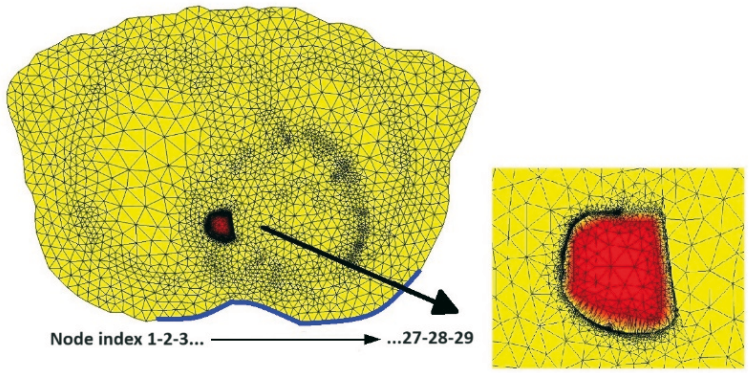

Fig. 5 Torso model and ischemic region in the left ventricle (Ischemia 2). The torso potential results are displayed for the nodes located along the chest boundary line (dark line) as a function of the node index.

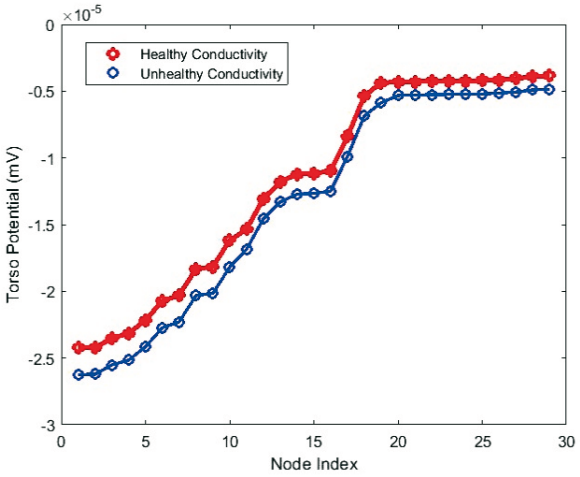

Fig. 6 Torso potentials predicted at the epicardial nodes with isotropic heart tissue and healthy and unhealthy (ischemic) conductivities (Ischemia 2).

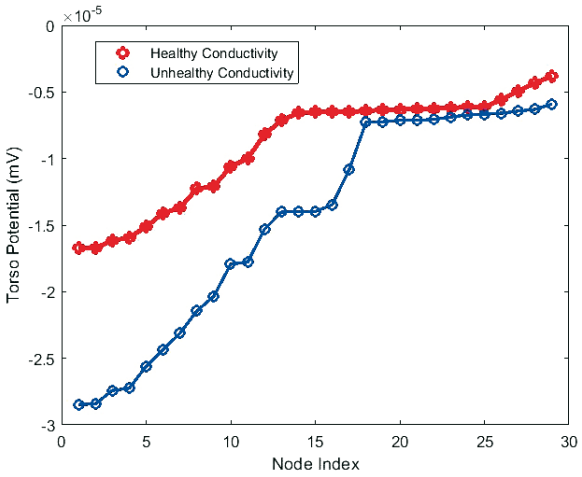

Fig. 7 Torso potentials predicted at the epicardial nodes with anisotropic heart tissue and healthy and unhealthy (ischemic) conductivities (Ischemia 2).

The third example (Ischemia 3, Fig. 8) involves an ischemic region in the right ventricle. Compared to the first two cases, the ischemic conductivity makes a smaller difference for the potentials read close to the sagittal plane both in isotropic (Fig. 9) and anisotropic (Fig. 10) cases. The difference is more pronounced at the leads away from the sagittal plane.

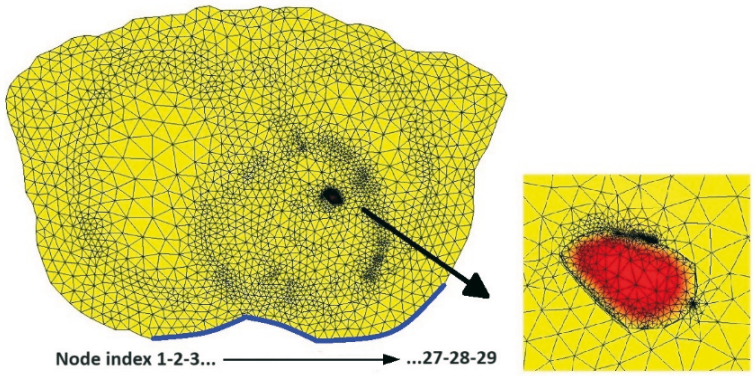

Fig. 8 Torso model and ischemic region in the right ventricle (Ischemia 3). The torso potential results are displayed for the nodes located along the chest boundary line (dark line) as a function of the node index.

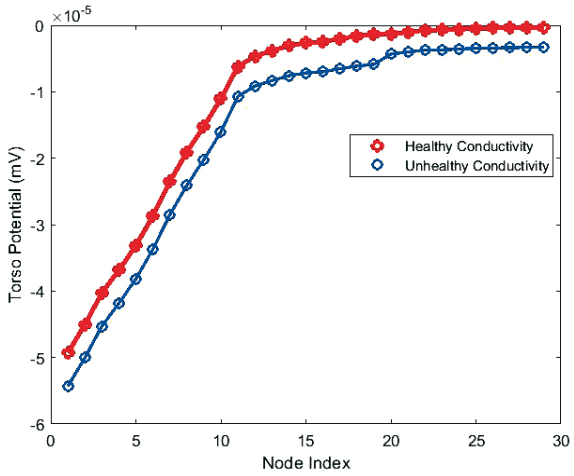

Fig. 9 Torso potentials predicted at the epicardial nodes with isotropic heart tissue and healthy and unhealthy (ischemic) conductivities (Ischemia 3).

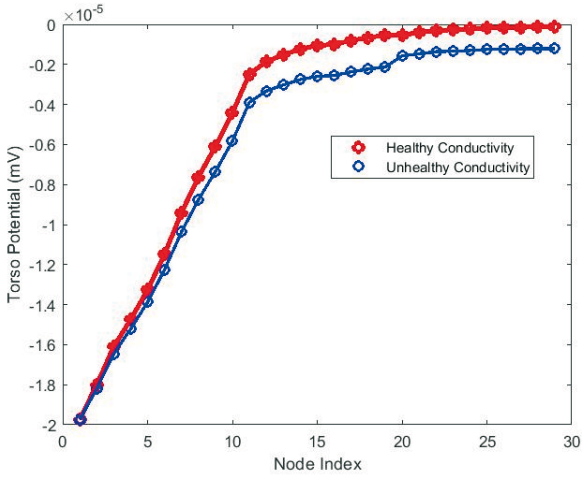

Fig. 10 Torso potentials predicted at the epicardial nodes with anisotropic heart tissue and healthy and unhealthy (ischemic) conductivities (Ischemia 3).

4. Discussion and Conclusions

FEM is widely used in various subfields of biomedical engineering such as orthopaedic biomechanics [31, 32], biofluid mechanics [33, 34], biomaterials [35, 36], and electrophysiology. With advancements in computer technology, computationally more complex but more accurate methods are proposed for forward cardiology problems, where more realistic physical properties are employed to model cardiac tissue, and for inverse cardiology problems, where FEM optimisation is achieved through gradient methods [37], artificial neural networks [38, 39], and genetic algorithms [40]. We believe that studies such as those presented here are useful small steps towards the more accurate FEM simulation of heart electrophysiology.

In this study, we have numerically investigated the effect of ischemic conductivity on the torso potentials for three different numerically constructed ischemia cases. To the best of our knowledge, this is the first study that evaluates the relevance of ischemic conductivity in numerical heart simulations.

We have observed that the torso potentials are affected differently depending on the size and location of the ischemic region. Larger ischemic regions that are closer to the pericardial (chest) leads cause a larger depression in the torso potentials.

Taking the ischemic conductivity into account can cause significant changes in the torso potentials. The magnitude of this change also depends on the size and location of the ischemic region. We have observed that the change is more pronounced if the ischemic region is larger and closer to the posterior of the heart (such as in the Ischemia 1 case). In other words, the larger the "heart material" between the ischemic region and the leads, the stronger is the effect of ischemic conductivity.

The anisotropy of the conductivity has a strong influence on the torso potentials. Ischemic conductivity has a greater effect on the torso potentials if the anisotropy of myocardium is taken into account. Depending on the size and the location of the ischemic region, anisotropic ischemic conductivity may lead to torso potentials that are twice as large as those produced by anisotropic healthy conductivity induced on the ischemic region. In the Ischemia 1 and 2 cases, this difference is percentage-wise smaller when isotropic conductivities are utilised. With isotropic conductivities, the difference may be smaller in magnitude but the shift in TMP is consistently towards higher magnitudes at each output point. A cross-comparison between the graphs reveals that the difference in the estimated torso potentials with isotropic-healthy conductivities and with anisotropic-unhealthy conductivities can be even more pronounced. Consequently, it can be argued that a significant improvement in the heart model can be achieved if ischemic conductivity and the associated anisotropy are simultaneously taken into account in the model.

In an entirely healthy heart, the torso potentials should read as exactly zero during the ST phase of ECG. In the case of ischemia, the difference in the TMP of the healthy and ischemic tissues forms a distributed dipole across their common boundary, which acts as a current source. The magnitude of the dipole is related to ∇V_m per equation (4). The length of the boundary (i.e. the size of the ischemic region) is a determinant of the cumulative strength of the source. These factors, along with the location of the ischemic region, determine the level of torso potentials. In general, the magnitude of the ST shift is relatively low, yet taking the ischemic conductivity into account makes a significant difference in the severity of the ST shift.

In this work, the transition of the TMP potential from the healthy to the ischemic region is given by the expression in equation (34). In the literature, different functional forms expressing a smooth transition from the healthy region to the unhealthy one are used [7-9], [41, 42]. It should be noted that the width of the transition zone h has a minimal effect on the problem outcome. The last term in Eq. 23 is the source term, ∇V_m where is integrated over the area of a closed strip surrounding the ischemia zone where it has a nonzero value. A smaller assumed h results in a larger ∇V_m value (hence a larger integrand value) but a smaller strip area (hence a smaller integration region). In contrast, a larger assumed h results in a smaller ∇V_m but a larger strip area. Consequently, the magnitude of the source term is related mainly to the value of ischemic V_m and the length of the ischemic zone boundary (hence the size of the ischemic region).

While the forward ECG problem is actually a three-dimensional problem, we performed a two-dimensional analysis in this work to deal with a moderate level of computational burden. Although we believe that the main conclusions are not going to change, it is possible to repeat this study on a three-dimensional model. The computational burden that comes with a three-dimensional simulation is significantly higher than we encountered in the current study, and a three-dimensional model requires proportionally higher computing resources. Another idealisation employed in this study is to use a generic torso model and conductivity values taken from the literature. In reality, torso geometries, as well as conductivity values, vary from one patient to another. We believe that the qualitative conclusions drawn from this study will remain largely intact, while its quantitative outcome may change with the above-mentioned factors, especially with variations in the torso geometry.

The computational setting established in this work can be used to research more clinically relevant problems. For example, if ischemic conductivity is taken into account, it may be possible for ischemia occurring in certain parts of the heart to be better located by solving the inverse problem of ECG with FEM. Similarly, again using the inverse problem, non-standard ECG lead spots can be identified on the chest to better locate the ischemia in the heart. In such an analysis, taking the ischemic conductivity into account may increase the solution accuracy of the problem.

REFERENCES

[1] Pullan, A.; Cheng, L.; Buist, M. Mathematically Modelling the Electrical Activity of the Heart, London: World Scientific Publishing Company, 2005. https://doi.org/10.1142/5859

[2] Wang, D. Finite Element Solutions to Inverse Electrocardiography, The University of Utah, United States, Ph.D. thesis, 2012.

[3] Stern, S. State of the Art in Stress Testing and Ischaemia Monitoring, Cardiac Electrophysiology Review 2002, 6(3), 204-208. https://doi.org/10.1023/A:1016364622124

[4] Pullan, A. A High Order Coupled Finite Element/Boundary Element Torso Model, IEEE Transactions on Biomedical Engineering 1996, 43(3), 292-298. https://doi.org/10.1109/10.486286

[5] Lines, G.; Buist, M.; Grøttum, P.; Pullan, A.; Sundnes, J.; Tveito, A. Mathematical models and numerical methods for the forward problem in cardiac electrophysiology, Computing and Visualization in Science 2003, 5(4), 215-239. https://doi.org/10.1007/s00791-003-0101-4

[6] Linge, B. S.; Sundnes, J.; Hanslien, M.; Lines, G. T. Numerical solution of the bidomain equations, Phil. Trans. R. Soc. 2009, 367(1895), 1931-1950. https://doi.org/10.1098/rsta.2008.0306

[7] Nielsen, B.; Lysaker, M.; Tveito, A. On the use of the resting potential and level set methods for identifying ischemic heart disease: An inverse problem, Journal of Computational Physics 2007, 220(2), 772-790. https://doi.org/10.1016/j.jcp.2006.05.040

[8] Johnston, B.; Johnston, P. Sensitivity analysis of ST-segment epicardial potentials arising from changes in ischemic region conductivities in early and late stage ischemia, Computers in Biology and Medicine 2018, 102, 288-299. https://doi.org/10.1016/j.compbiomed.2018.06.005

[9] Burton, B.; Aras, K.; Good, W.; Tate, J.; Zenger, B.; MacLeod, R. Image-based modeling of acute myocardial ischemia using experimentally derived ischemic zone source representations, Journal of Electrocardiology 2018, 51(4), 725-733. https://doi.org/10.1016/j.jelectrocard.2018.05.005

[10] Wei, C.; Valvano, J.; Feldman, M. 3D Finite Element Complex Domain Numerical Models of Electric Fields in Blood and Myocardium, in Proceedings of the 25th Annual International Conference of the IEEE EMBS, Cancun, Mexico, 2003.

[11] Henriquez, C. S. A Brief History of Tissue Models for Cardiac Electrophysiology, IEEE Transactions On Biomedical Engineering 2014, 61(5) 1457-1465. https://doi.org/10.1109/TBME.2014.2310515

[12] Clayton, R. H.; Panfilov, A. V. A guide to modeling cardiac electrical activity in anatomically detailed ventricles, Progress in Biophysics and Molecular Biology 2008, 96, (1-3), 19-43. https://doi.org/10.1016/j.pbiomolbio.2007.07.004

[13] Geneser, S. E.; Kirby, R. M.; MacLeod, R. S. Application of Stochastic Finite Element Methods to Study the Sensitivity of ECG Forward Modeling to Organ Conductivity, IEEE Transactions on Biomedical Engineering 2008, 55(1), 31 - 40. https://doi.org/10.1109/TBME.2007.900563

[14] Nezlobinsky, T.; Solovyova, O.; Panfilov, A.V. Anisotropic conduction in the myocardium due to fibrosis: the effect of texture on wave propagation, Scientific Reports 2020, 10(1), 1-12. https://doi.org/10.1038/s41598-020-57449-1

[15] Mani Aouadi, S.; Mbarki, W.; Zemzemi, N. Towards the modeling of the Purkinje/myocardium coupled problem: A well-posedness analysis, Journal of Computational and Applied Mathematics 2019, 351, 138-152. https://doi.org/10.1016/j.cam.2018.10.024

[16] Sundnes, J.; Terje Lines, G.; Cai, X. Computing the Electrical Activity in the Heart, Berlin, Springer, 2006.

[17] Hooks, D. A.; Trew, M. L. Construction and Validation of a Plunge Electrode Array for Three-Dimensional Determination of Conductivity in the Heart, IEEE Transactions on Biomedical Engineering 2008, 55(2), 626-635. https://doi.org/10.1109/TBME.2007.903705

[18] Johnston, P. R. A sensitivity study of conductivity values in the passive bidomain equation, Mathematical Biosciences 2011, 232(2), 142-150. https://doi.org/10.1016/j.mbs.2011.05.004

[19] Johnston, P. R. A nondimensional formulation of the passive bidomain equation, Journal of Electrocardiology 2011, 44(2), 184-188. https://doi.org/10.1016/j.jelectrocard.2010.11.015

[20] Ben-Shahar, O.; Zucker, S. W.; The Perceptual Organization of Texture Flow: A Contextual Inference Approach, IEEE Transactions on Pattern Analysis and Machine Intelligence 2003, 25(4), 401-417. https://doi.org/10.1109/TPAMI.2003.1190568

[21] Savadjiev, P.; Strijkers, G. J.; Bakermans, A. J.; Piuze, E.; Zucker, S. W.; Siddiqi, K. Heart wall myofibers are arranged in minimal surfaces to optimize organ function, PNAS 2012, 109(49), 9248-9253. https://doi.org/10.1073/pnas.1120785109

[22] Savadjiev, P.; Zucker S. W.; Siddiqi, K. On the Differential Geometry of 3D Flow Patterns: Generalized Helicoids and Diffusion MRI Analysis, IEEE 11th International Conference on Computer Vision, Rio de Janeiro, Brazil, 2007. https://doi.org/10.1109/ICCV.2007.4409086

[23] Stinstra, J. G.; Shome, S.; Hopenfeld B.; MacLeod, R.; Modelling passive cardiac conductivity during ischaemia, Medical and Biological Engineering and Computing 2005, 43(6), 776-782. https://doi.org/10.1007/BF02430957

[24] Ruud, T. S.; Nielsen, B. F.; Lysaker, M.; Sundnes, J. A Computationally Efficient Method for Determining the Size and Location of Myocardial Ischemia, IEEE Transactions on Biomedical Engineering 2009, 56(2), 263-272. https://doi.org/10.1109/TBME.2008.2009068

[25] Geneser, S. E.; Choe, S.; Kirby, R. M.; MacLeod, R. S. The Influence of Stochastic Organ Conductivity in 2D ECG Forward Modeling: A Stochastic Finite Element Study, 27th Annual Conference in Engineering, Medicine, and Biology, Shanghai, China, 2005. https://doi.org/10.1109/IEMBS.2005.1615736

[26] Klepfer, R. N.; Johnson R.; Macleod, S. R. The Effects of Inhomogeneities and Anisotropies on Electrocardiographic Fields: A 3-D Finite-Element Study, IEEE Transactions on Biomedical Engineering 1997, 44(8), 706-719. https://doi.org/10.1109/10.605427

[27] MacLachlan, M. C.; Nielsen, B. F.; Lysaker, M.; Tveito, A. Computing the Size and Location of Myocardial Ischemia Using Measurements of ST-Segment Shift, IEEE Transactions on Biomedical Engineering 2006, 53(6), 1024-1031. https://doi.org/10.1109/TBME.2005.863928

[28] Hopenfeld, B.; Stinstra, J.; Macleod, R. Mechanism for ST Depression Associated with Contiguous Subendocardial Ischemia, Journal of Cardiovascular Electrophysiology 2004, 15(10), 1200-1206. https://doi.org/10.1046/j.1540-8167.2004.04072.x

[29] Miller, W. T.; Geselowitz, D. B. Simulation studies of the electrocardiogram. II. Ischemia and infarction, Circulation Research 1978, 43(2), 315-323. https://doi.org/10.1161/01.RES.43.2.315

[30] MacLachlan, M.; Sundnes, J.; Lines, G. Simulation of ST segment changes during subendocardial ischemia using a realistic 3-D cardiac geometry, IEEE Transactions on Biomedical Engineering 2005, 52, (5), 799 - 807. https://doi.org/10.1109/TBME.2005.844270

[31] Verim, O. Development and Investigation of the Mechanical Behaviour of Circular External Fixators during the Gait Cycle, Transactions of FAMENA 2022, 46(1), 81-90. https://doi.org/10.21278/TOF.461029121

[32] Ghosh, R.; Chanda, S.; Chakraborty, D. Application of finite element analysis to tissue differentiation and bone remodelling approaches and their use in design optimization of orthopaedic implants: A review, International Journal for Numerical Methods in Biomedical Engineering 2022, 38(10), e3637. https://doi.org/10.1002/cnm.3637

[33] Lopes, D.; Puga, H.; Teixeira, J.; Lima, R. Blood flow simulations in patient-specific geometries of the carotid artery: A systematic review, Journal of Biomechanics 2020, 111, 1-17. https://doi.org/10.1016/j.jbiomech.2020.110019

[34] Lopes, D.; Agujetas, R.; Puga, H.; Teixeira, J.; Lima, R.; Alejo, J.P.; Ferrera, C. Analysis of finite element and finite volume methods for fluid-structure interaction simulation of blood flow in a real stenosed artery, International Journal of Mechanical Sciences 2021, 207, 106650. https://doi.org/10.1016/j.ijmecsci.2021.106650

[35] Leder, J.; Lulic, T. J.; Smojver, I. Stress Analysis of a Single Root Tooth Loaded with Orthodontic Forces, Transactions of FAMENA 2009, 33(4), 9-18.

[36] Thiyagu, S.; Bharathi, T.D.; Soundarraj, A.; Sriram, K.; Venkatraman, S.; Krishna, A.V.R. Finite Element Analysis Based Comparison of Biomaterials Used in Femur Bone Replacements, Trends in Biomaterials and Artificial Organs 2021, 35(4), 354-359.

[37] Hamed, K.; Mustafa K. Ü. A novel iterative finite element optimisation method of solving inverse problem of electrocardiography to localise ischemic region on the heart, Maejo International Journal of Science and Technology 2022, 16(3), 275-290.

[38] Xie, J.; Yao, B. Physics-constrained deep learning for robust inverse ECG modeling, IEEE Transactions on Automation Science and Engineering. 2022, 20(1), 151 - 166. https://doi.org/10.1109/TASE.2022.3144347

[39] Vijayan, S.; Parameshwaran Pillai, T. Application of a Machine Learning Algorithm in a Multi Stage Production System, Transactions of FAMENA 2022, 46 (1), 91-102. https://doi.org/10.21278/TOF.461033121

[40] Sedlar, D.; Lozina, Ž.; Vučina, D. Comparison of Genetic and Bees Algorithms in the Finite Element Model Update, Transactions of FAMENA 2011, 35(1), 1-12.

[41] Johnston, P. A finite volume method solution for the bidomain equations and their application to modeling cardiac ischemia, Computer Methods in Biomechanics and Biomedical Engineering 2010, 13, (2), 157-170. https://doi.org/10.1080/10255840903067072

[42] Johnston, B.; Coveney, S.; Chang, T.; Johnston, P.; Clayton, R. Quantifying the effect of uncertainty in input parameters in a simplified bidomain model of partial thickness ischemia, Medical & Biological Engineering & Computing 2018, 56(5), 761-780. https://doi.org/10.1007/s11517-017-1714-y

Submitted: 02.01.2023

Accepted: 22.11.2023

Hamed Kaghazchi*
Baku Engineering University
Faculty of Engineering
Hasan Aliyev St. 120, AZ0101,
Baku, Azerbaijan
Mustafa Kerem Ün
Cukurova University
Faculty of Engineering
Balcalı, Sarıçam, 01330,
Adana, Turkey
*Corresponding author:
hkaghazchi@beu.edu.az